Controlling competing interactions at oxide interfaces: Enhanced anisotropy in La$_{0.7}$Sr$_{0.3}$MnO$_3$ films via interface engineering

J.-S. Lee,[1,*] D. A. Arena,[2] T. S. Santos,[3,4] C. S. Nelson,[2] S. I. Hyun,[5] J. H. Shim,[5] and C.-C. Kao[1]

[1]*Stanford Synchrotron Radiation Lightsource, SLAC National Accelerator Laboratory, Menlo Park, California 94025, USA*
[2]*National Synchrotron Light Source, Brookhaven National Laboratory, Upton, New York 11973, USA*
[3]*Western Digital Corporation, San Jose, California 95138, USA*
[4]*Center for Nanoscale Materials, Argonne National Laboratory, Argonne, IL 60439, USA*
[5]*Department of Chemistry, Pohang University of Science and Technology, Pohang 790-784, S. Korea*

We investigated thin La$_{0.7}$Sr$_{0.3}$MnO$_3$-SrTiO$_3$ heterostructures, where the band alignment is engineered by a variation of La/Sr stoichiometry only at the interface. In thin films, the engineered interface leads to an enhancement of the reversed spin configuration that mimics bulk behavior. Microscopically, this enhancement is closely connected with an increased magnetic anisotropy as well as intercoupling between an e_g orbital reconstruction and a corresponding anisotropic lattice fluctuation. Furthermore, a *reentrant*-type behavior, triggered by this intercoupling, is observed in the remanent spin state. This microscopic perspective leads to insights on developing new strategies for maintaining bulk-like properties even in very thin La$_{0.7}$Sr$_{0.3}$MnO$_3$ heterostructures.

PACS number(s): 75.47.Lx, 75.30.Kz, 75.70.Cn

The remarkable tunability of the physical properties of complex oxides motivates extensive and ongoing research on heterostructures, both to investigate new phenomena[1–4] and to exploit such phenomena in device applications.[5–7] Moreover, in oxide heterostructures, additional control mechanisms are available, such as deliberately altering the interfacial polar discontinuity to modify the physical properties of thin-film structures.[8–12] Among the perovskite class of oxides, mixed-valence manganites exhibit unusually complex phase diagrams,[13] and La$_{1-x}$Sr$_x$MnO$_3$ is extensively incorporated into a wide variety of spin-dependent electronic devices.[14,15] In the bulk, variations in the Sr doping (x) produce a complex phase diagram,[16] with the concomitant changes in band structures (e.g., band width or gap) and orbital character.[17–19] Hence, in La$_{1-x}$Sr$_x$MnO$_3$-based heterostructures, the Sr doping level is a controlling parameter for tuning various phenomena. Meanwhile, La$_{1-x}$Sr$_x$MnO$_3$ with a doping $x \sim 0.3$ is a popular choice for spin-dependent heterostructures and devices[6] as La$_{0.7}$Sr$_{0.3}$MnO$_3$ is a wide-band half-metallic ferromagnet[20] with a high Curie temperature (T_c). In LSMO-based devices (hereafter, "LSMO" refers specifically to La$_{0.7}$Sr$_{0.3}$MnO$_3$), the wide gap insulator SrTiO$_3$ (STO) is a very common choice for tunnel barriers.

However, in the resulting composite heterostructure, interfacial strain, charge transfer, symmetry breaking, and other effects can lead to new phenomena.[1–5] An example is the recently identified anomalous spin configuration in LSMO-STO heterostructures—where the near-surface region of the LSMO film can adopt a reversed remanent state that is opposite to the direction of the applied magnetic field.[21] An additional example is the induced magnetic moment of Ti d electrons via superexchange with Mn in LSMO-STO heterostructures.[22,23] Ideally, LSMO is expected to have a 70%/30% charge distribution of Mn^{3+}/Mn^{4+}. However, the natural interface in LSMO/STO heterostructures [Fig. 1(a)] (i.e., the interface without a deliberate introduction of a different La/Sr ratio) has an enriched Mn^{3+} concentration.

This suggests that charge accommodation at the interface may be an important mechanism in the formation of the reversed magnetic state. With this as the background, in this paper we directly address the effect of interfacial properties by deliberately introducing an engineered interface between LSMO and STO that is controlled by (La/Sr) stoichiometry at the first La$_{1-x}$Sr$_x$MnO$_3$ unit cell (UC), termed the δ layer, where the Sr doping is varied from $x_\delta = 0.15$ to $x_\delta = 0.67$ [Fig. 1(b)]. Using comprehensive synchrotron studies, we found an enhancement of the reversed spin configuration, mimicking bulk-like phenomena even in thin films. Microscopically, spectroscopy and scattering studies reveal that this enhancement is closely connected with an enhanced magnetic anisotropy generated via intercoupling between a reconstructed Mn e_g orbital and a corresponding structural fluctuation of MnO$_6$ octahedra. Moreover, such intercoupling triggers a *reentrant* type behavior in the remanent spin state.

As LSMO is metallic and STO is a wide-band insulator, the LSMO-STO heterostructure ideally experiences a large band offset at the interface, which is accommodated by interfacial band bending in the conduction and valence bands of the insulator. Therefore, a different band structure of the δ layer in the engineered structure leads to a modified band-bending effect [Fig. 1(c), schematic pictures]. As mentioned above, the natural (i.e., unmodified) interface already has an enriched Mn^{3+} concentration. Therefore, the additional band modification introduced by varying the La/Sr ratio at the interface is expected to be especially pronounced for the highly doped δ layer ($x_\delta = 0.67$).

To gain insight into the effects introduced by such interfacial engineering, we performed a first-principles calculation (i.e., density functional theory calculation with the full-potential linearized augmented plane wave[24]) on model structures—LSMO(6 UC)/STO (TiO$_2$ termination) and LSMO(5 UC)/La$_{1-x}$Sr$_x$MnO$_3$(1 UC)/STO (TiO$_2$ termination) with the δ layer. In the natural LSMO-STO interface, the layer-resolved density of states (DOS) reveal appreciable band
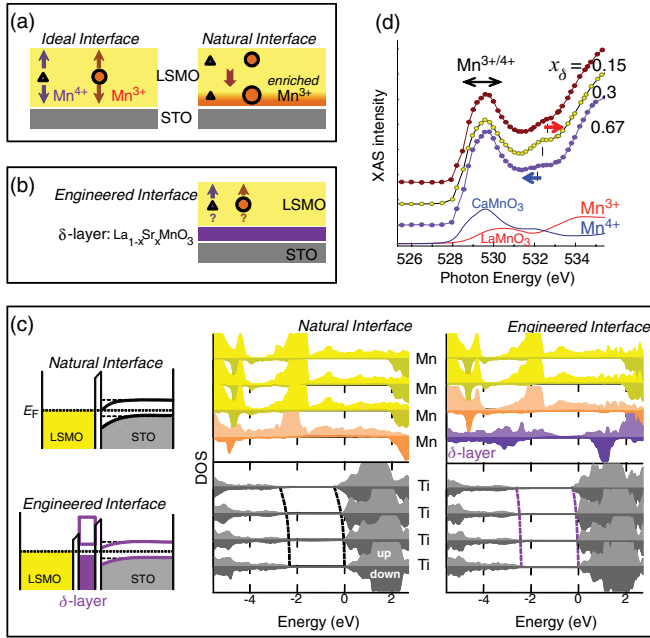
FIG. 1. (Color online) (a) Representations of Mn valence states in ideal (abrupt) and natural interfaces. (b) Engineered interfaces. (c) Schematics of band alignment on natural interface and engineered interface. Plots of the layer-resolved DOS in LSMO/STO(001) and LSMO/La$_{0.5}$Sr$_{0.5}$MnO$_3$(1 UC)/STO heterostructures that represent the natural and engineered interface, respectively. Yellow, orange, and violet color codes for the DOS are for bulk-like Mn in LSMO, enriched Mn^{3+}, and Mn in the δ layer, respectively. Dashed lines indicate the band bending effect, which is obtained from the valence band maximum and conduction band minimum. (d) Oxygen XAS spectra of the engineered heterostructures with $x_\delta = 0.15$, 0.3, and 0.67. The reference spectra, CaMnO$_3$ and LaMnO$_3$, are selected to represent the Mn^{4+} and Mn^{3+} states, respectively.

bending [Fig. 1(c)] with a charge transfer from LSMO layers to interfacial STO layers. The interfacial Ti 3d bands are partially occupied due to the charge transfer at the interface. The electrons in LSMO layers are driven to the interface due to the electron repulsion in the metallic region. Note that the Mn 3d bands shift downward upon approaching to the interface. Accordingly, the Mn 3d orbital occupation also increases near the interface and surface, resulting in an enhancement of the Mn^{3+} concentration. In the highly-Sr-doped interface simulated with $x_\delta = 0.5$,[25] the band-bending becomes much weaker (see the dashed line in the DOS plot). On either side of the δ layer, the adjacent LSMO or STO layers retain an electronic structure much more similar to their respective bulk parent compounds than is the case in the natural LSMO/STO interface. As the TiO$_2$ layer faces the highly doped La$_{0.5}$Sr$_{0.5}$O layer (lower carrier density), charge transfer to the STO layer is much reduced. Furthermore, the La$_{0.5}$Sr$_{0.5}$O layer also effectively buffers the LSMO layers, leading to a nearly invariant Mn 3d occupation. When the Sr doping is larger than 0.6, La$_{1-x}$Sr$_x$MnO$_3$ is in an insulating phase,[18] hence buffering the band offset between the metallic LSMO and the insulating STO.

We explore such effects experimentally using a combination of advanced thin-film growth techniques and synchrotron-based characterization. Engineered heterostructures, LSMO(19 UC)/La$_{1-x}$Sr$_x$MnO$_3$(1 UC), were grown by molecular beam epitaxy deposition on a TiO$_2$-terminated substrate (B-site) under conditions known to produce epitaxial films with near-perfect interfaces.[26,27] The total film thickness of 20 UC ($\sim$80 Å) was selected to enable sampling of the interfacial region with total electron yield (TEY) used in the spectroscopic measurements. TEY has a probe depth of $50 \sim 100$ Å. In the UC δ layer, the Sr concentration $x_\delta = 0.15$, 0.3, and 0.67.

The additional 1 UC δ layer effectively changes the hole concentration at the interface, which may cause an additional effect via a modified polar discontinuity.[6] To probe an interfacial modification in these engineered heterostructures, we carried out x-ray absorption spectroscopy (XAS) at the O K edge [Fig. 1(d)]. As the thickness of the LSMO film and the deliberately modified interfaces are 19 UC and 1 UC, respectively, in this engineered heterostructure, the overall spectral shape is dominated by the LSMO film. Nevertheless, a small difference, originating in the modified interface, is observed. Note that there may be changes to the Mn oxidation state that arise from oxygen vacancies, however oxygen deficiency seems to be either zero or below the experimental detection limit. The implication of the differences in the spectra can be determined by comparison with reference spectra: CaMnO$_3$ (i.e., only Mn^{4+} valence) and LaMnO$_3$ (Mn^{3+}). In comparison with $x_\delta = 0.3$, the spectral features of the low- and highly-doped samples around $E = 532.4$ eV move to a higher (more Mn^{3+}) and a lower (more Mn^{4+}) photon energy, respectively. We also confirmed that the Mn L edge XAS were consistent with the oxygen spectral features. The XAS indicates that the $x_\delta = 0.15$ and $x_\delta = 0.67$ samples have modified the concentrations of Mn^{3+} and Mn^{4+}, which in turn may affect the interfacial band modification.

We now investigate the relationship between the engineered interface and the magnetic reversal behavior of LSMO, using Mn $L_{2,3}$ x-ray magnetic circular dichroism (XMCD). The experiments were carried out at beamline U4B at the National Synchrotron Light Source (NSLS). We employed two modes for controlling the external magnetic field (H).[21] One mode of control was via a holding H field (h XMCD)—saturation state—and the other employed a pulsed H field (p XMCD)—remanent state. The $x_\delta = 0.3$ (unmodified interface) behaves as expected for LSMO films on STO, resulting in the reversed dichroic signals [Fig. 2(a)], which implies an antiparallel remanent spin configuration relative to the H field. In addition, temperature-dependent p XMCD spectra reveal that the temperature onset of the reversed remanent magnetic state (T_a) is $\sim$35 K. Considering prior results,[21] T_a depends on the thickness of an intermediate layer (IL) with an enriched Mn^{3+} concentration. In comparison to the IL thickness in a thick LSMO(90 UC)/STO heterostructure; $T_a \sim 240$ K,[28] which is expected to behave in a bulk-like fashion, the IL in this thin (20 UC) film must be thinner than in the 90 UC case. The IL is expected to be about 16 Å for such a low T_a. In the $x_\delta = 0.15$ case, the reversal behavior still was apparent [Fig. 2(b)], but now T_a increases to $\sim$55 K. Relative to the $x_\delta = 0.3$ case, the IL thickness is expected to be larger, which is consistent with the increased Mn^{3+} concentration intentionally introduced at the interface.
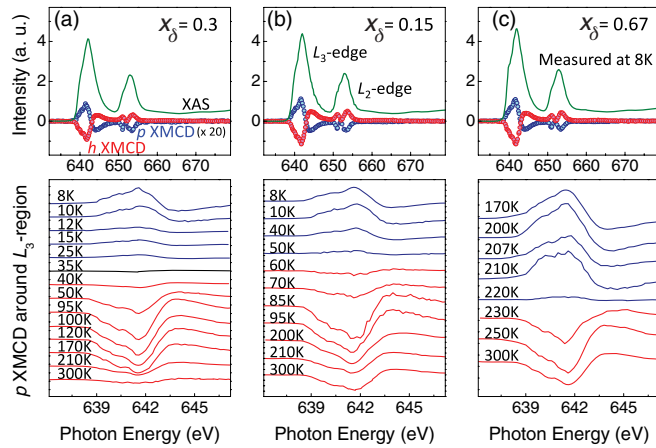
FIG. 2. (Color online) X-ray magnetic circular dichroism on LSMO(19 UC)/La$_{1-x}$Sr$_x$MnO$_3$(1 UC)/STO[001] heterostructures with (a) $x = 0.15$, (b) 0.3, and (c) 0.67. Two different H field modes: h XMCD and p XMCD (top), and temperature dependent p XMCD around Mn L_3-edge region (bottom).

FIG. 3. (Color online) (a) T dependence of H_c behavior on LSMO(19 UC)/La$_{0.33}$Sr$_{0.67}$MnO$_3$(1 UC)/STO[001]. Dashed and solid lines are guide to the eye. (b) p XMCD around Mn L_3 region of the $x_\delta = 0.67$ case within full temperature range. Arrows denote transitions. (c) Variations in intensities at L_3 edge. The dashed lines and arrows are guides to the eye. The inset schematic indicate the character of the e_g orbital.

Remarkably, T_a increases to $\sim$220K [Fig. 2(c)] in the $x_\delta = 0.67$ sample. If the origin of such increase is a thicker IL, the IL must increase by more than $\sim$3 UC to account for the increase in T_a. However, as in the $x_\delta = 0.15$ case, only 1 UC was modified at the interface, and $x_\delta = 0.67$ decreases the Mn^{3+} concentration at the interface. Moreover, the bulk magnetization for the highly doped interface sample, measured by a superconducting quantum interference device (SQUID), shows an enhancement of the total moment, even though the spin moment of the Mn^{4+} state is lower than that of the Mn^{3+} spin moment. Therefore, another mechanism must cause the modification of these magnetic behaviors for $x_\delta = 0.67$.

The enriched Mn^{3+} state in the IL undergoes a reconstruction of the anisotropic e_g orbital ($d_{3z^2-r^2}$),[29] which is associated with the reversal of the remanent magnetization.[21] According to the La$_{1-x}$Sr$_x$MnO$_3$ phase diagram[18] the e_g orbital in $0.6 < x < 0.9$ region preferentially adopts a $d_{3z^2-r^2}$ character. Therefore, if the highly doped $x_\delta = 0.67$ layer reinforces the orbital anisotropy, the magnetic properties may also be modified. As the orbital anisotropy is a key determinant of magnetic anisotropy, we investigated the magnetic anisotropy via magnetic hysteresis loop measurements. Figure 3(a) clearly shows a change in the magnetic coercivity (H_c) of the $x_\delta = 0.67$ case. We observed an increase in the H_c behavior below 220 K, consistent with a reconstruction of the e_g orbital, which is distinguishable from a thermal effect (i.e., phonon contribution) below the sample's T_c. As the increased $d_{3z^2-r^2}$ population is intentionally introduced at the interface, the magnetic exchange interaction induced by the anisotropic orbital population overcomes the thermal interaction at T_a.

Interestingly, we observe an additional anomaly of H_c around 110 K which is similar to the structural transition temperature (T_s) of STO.[30,31] This points to an additional connection between the structural and magnetic degrees of freedom, which we monitor more closely with p XMCD across a wide temperature range [Fig. 3(b)]; the temperature-dependent p XMCD intensity around the Mn L_3 edge is displayed in Fig. 3(c). The p XMCD signal reverses at T_a,
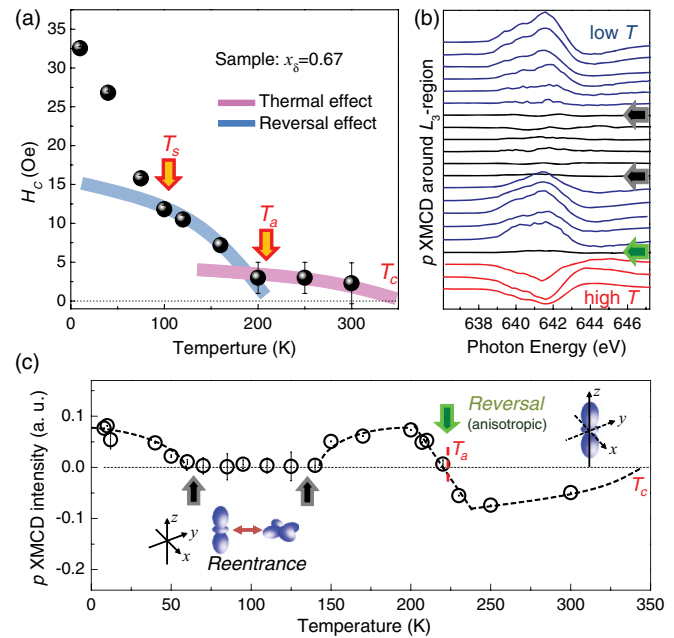
disappears in the vicinity of T_s, and reemerges below 70 K, indicating a *reentrant* type of behavior. A similar reentrant behavior was observed in a much thicker LSMO(90 UC)/STO heterostructure.[28] Also, T_a in this 20 UC, $x_\delta = 0.67$ case is similar to the significantly thicker film, implying that the deliberate introduction of the additional Mn^{4+} at the interface generates bulk-like behavior in the much thinner film. This bulk-like transition temperature in the 20 UC film parallels the preservation of bulk-like electronic structure and reduced band bending illustrated in the layer-resolved DOS calculations shown in Fig. 1(c). However, in the case of the 90 UC film with the unmodified interface, the p XMCD intensity merely decreases around T_s, rather than experiencing a complete collapse as is see in Figs. 3(b) and 3(c). As this reentrant behavior is closely associated with the electronic and orbital structure at the interface, the effects of the substrate structural anomaly at $\sim$110 K is more pronounced in the 20 UC sample.

As the magnetic behavior of the LSMO(90 UC)/STO sample and the $x_\delta = 0.67$ sample are quite similar, we monitor the structural response of the LSMO film, concentrating on the 90 UC sample. Also, we confirmed that the in-plane strain is relieved as the interfacial Sr doping (x) is increased. Figure 4(a) presents the positions of the STO and LSMO (002) (out-of-plane) and (112) (includes in-plane components) reflections. If the orbital fluctuation in the LSMO occurs at the interface, any accompanying variation of the lattice parameters is expected to be be very weak. For enhancing such small variations, we plot in Fig. 4(b) the ratios between the LSMO and STO 2θ positions. Below 240 K (i.e., T_a of this thick system), we observe an increase in the out-of-plane lattice parameter.
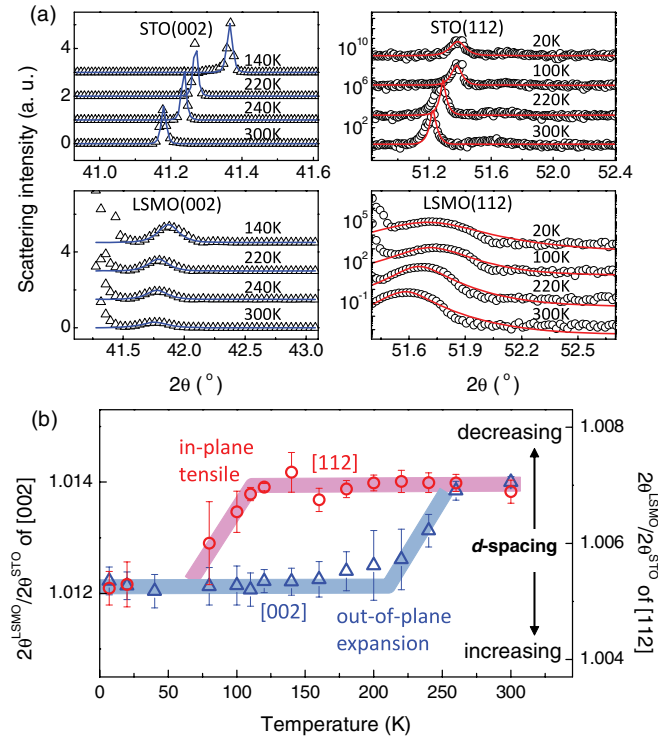
FIG. 4. (Color online) XRD results on LSMO(90 UC)/STO[001] as a function of temperature. (a) Bragg peaks on STO(002) and STO(112): top, and LSMO(002) and LSMO(112): bottom. The solid lines are fits to the data. (b) T dependence of the ratios between the 2θ positions of STO(002) and LSMO(002) (left axis). The ratio of (112) positions (right axis). The thick solid lines are added as a guide to the eye.

This implies that the out-of-plane expansion is compensated by the in-plane compression, leading to a reconstructed and anisotropic $d_{3z^2-r^2}$ in the MnO$_6$ octahedra, which is consistent with previous work.[21] Note that band-structure calculations confirm the effect of strain on the Mn energy levels and orbital

occupation. Upon cooling, the structural distortion along the in-plane direction becomes tensile around $T \sim 110$ K, which weakens the tendency to populate the $d_{3z^2-r^2}$ orbitals at the interface and increases the population of the $d_{x^2-y^2}$ orbitals. As a result, the interface may experience an orbital fluctuation ($d_{3z^2-r^2} \leftrightarrow d_{x^2-y^2}$) around T_s [Fig. 3(c), inset], resulting in a collapse of the reversed p XMCD signal. Below $T \sim 70$ K, the variation of the film/substrate ratio stabilizes, weakening the lattice fluctuation and reestablishing the p XMCD signal. This is also in agreement with a recent transport measurements on La$_{0.53}$Sr$_{0.47}$MnO$_3$/SrTiO$_3$ heterostructures,[32] where the manganite resistivity develops a pronounced cusp across a wide temperature range corresponding to a phonon softening transition in the STO.

By carefully engineering the (La/Sr) doping ratio at the interface, we controlled not only the stoichiometry, but also the strong intercoupling between the orbital, lattice, and spin degrees of freedom. In particular, this kind of interface engineering can generate bulk-like behaviors, even in thin films. Moreover, the insights obtained from the mechanisms associated with and possibly responsible for these effects offer a considerable potential for application to oxide thin-film devices, with the added possibility of the appearance of new forms of spin coupling and device functionality. Finally, the evidence of control over orbital degrees of freedom at the interface of the heterostructure offers a rich opportunity for detailed experimental investigations and theoretical interpretations.

---

*To whom correspondence should be addressed: jslee@slac.stanford.edu

[1] A. Ohtomo and H. Y. Hwang, Nature (London) **427**, 423 (2004).

[2] J. Chakhalian *et al.*, Nat. Phys. **2**, 244 (2006).

[3] Y. Tokura and H. Y. Hwang, Nat. Mater. **7**, 694 (2008).

[4] J. Mannhart and D. G. Schlom, Science **327**, 1607 (2010).

[5] S. M. Wu *et al.*, Nat. Mater. **9**, 756 (2010).

[6] T. Yajima, Y. Hikita, and H. Y. Hwang, Nat. Mater. **10**, 198 (2011).

[7] Y. Yamada *et al.*, Science **332**, 1065 (2011).

[8] N. Nakagawa, H. Y. Hwang, and D. A. Muller, Nat. Mater. **5**, 204 (2006).

[9] Y. Hotta, T. Susaki, and H. Y. Hwang, Phys. Rev. Lett. **99**, 236805 (2007).

[10] M. Minohara, R. Yasuhara, H. Kumigashira, and M. Oshima, Phys. Rev. B **81**, 235322 (2010).

[11] G. Singh-Bhalla *et al.*, Nat. Phys. **7**, 80 (2011).

[12] H. W. Jang *et al.*, Science **331**, 886 (2011).

[13] J. M. D. Coey *et al.*, Adv. Phys. **48**, 167 (1999).

[14] Y. Lu, X. W. Li, G. Q. Gong, G. Xiao, A. Gupta, P. Lecoeur, J. Z. Sun, Y. Y. Wang, and V. P. Dravid, Phys. Rev. B **54**, R8357 (1996).

[15] J. M. De Teresa, A. Barthelemy, A. Fert, J. P. Contour, R. Lyonnet, F. Montaigne, P. Seneor, and A. Vaures, Phys. Rev. Lett. **82**, 4288 (1999).

[16] E. Dagotto, T. Hotta, and A. Moreo, Phys. Rep. **344**, 1 (2001).

[17] Y. Fujimori, J. Phys. Chem. Solids **53**, 1595 (1992).

[18] Y. Tokura, Rep. Prog. Phys. **69**, 797 (2006).

[19] E. Benckiser *et al.*, Nat. Mater. **10**, 189 (2011).

[20] J.-H. Park *et al.*, Nature (London) **392**, 794 (1998).

[21] J.-S. Lee, D. A. Arena, P. Yu, C. S. Nelson, R. Fan, C. J. Kinane, S. Langridge, M. D. Rossell, R. Ramesh, and C. C. Kao, Phys. Rev. Lett. **105**, 257204 (2010).

[22] F. Y. Bruno *et al.*, Phys. Rev. Lett. **106**, 147205 (2011).

[23] J. Garcia-Barriocanal *et al.*, Nat. Commun. **1**, 82 (2010).

[24] P. Blaha, K. Schwarz, G. K. H. Madsen, D. Kvasnicka, and J. Luitz, WIEN2K, an augmented plane wave + local orbitals program for calculating crystal properties (Technische Universität, Wien, Austria, 2001).

[25] We use a $\sqrt{2} \times \sqrt{2}$ supercell to describe the insulating layer with Mn^{3+} and Mn^{4+} in the $La_{0.5}Sr_{0.5}MnO_3\delta$ layer.

[26] T. S. Santos, S. J. May, J. L. Robertson, and A. Bhattacharya, Phys. Rev. B **80**, 155114 (2009).

[27] The interfacial stoichiometry, estimated via additional XAS scans and modeling (not shown), show the interfacial Mn valence to be close to the nominal composition, and within the expected growth uncertainty ($\sim \pm 5\%$).

[28] J.-S. Lee *et al.*, J. Phys. D: Appl. Phys. **44**, 245002 (2011).

[29] A. Tebano *et al.*, Phys. Rev. Lett. **100**, 137401 (2008).

[30] K. W. Blazey, Phys. Rev. Lett. **27**, 146 (1971).

[31] J. F. Scott, Rev. Mod. Phys. **46**, 83 (1974).

[32] Y. Segal, K. F. Garrity, C. A. F. Vaz, J. D. Hoffman, F. J. Walker, S. Ismail-Beigi, and C. H. Ahn, Phys. Rev. Lett. **107**, 105501 (2011).